Copyright © 2012 Tech Science Press CMES, vol.89, no.5, pp.389-416, 2012

Nonlinear Elastic-Plastic Analysis of Composite Members of High-Strength Steel and Geopolymer Concrete

Mark Andrew Bradford[1] **and Yong-Lin Pi**[1]

Abstract: This paper is devoted to the development of a finite composite beam element for the nonlinear elastic-plastic analysis of composite high strength steel and geopolymer concrete members. For this, geometric nonlinearity is derived using a special orthogonal rotation matrix, so that scalar product of vectors is preserved during rotation from the initial configuration to a deformed configuration and rigid body movements are excluded from the finite strains. The material nonlinearities of the geopolymer concrete are based on constitutive models in association with its axial stress-strain relationship that is consistent with the experimental results. To consider the slip due to possible partial shear connection of the bolts, the slip displacement between the high strength steel and geopolymer concrete components is treated as an independent degree-of-freedom. The effects of the nonlinearities and slip on the deformations, strains, stress resultants, and stiffness are thus combined together in the finite element formulation. The comparisons with experimental results demonstrate that the finite composite beam element is efficient, effective, and accurate. The finite composite beam element provides the much needed computer modeling of the structural mechanics and behaviour of high strength steel and geopolymer concrete members with bolted shear connectors, which are environmentally sustainable because they reduce the greenhouse emissions and can be deconstructed and recycled at the end of their service life.

Keywords: composite member, elastic-plastic analysis, finite element, geopolymer concrete, high strength steel, nonlinear, slip, interface.

1 Introduction

This paper is concerned with the development of a finite composite beam element for the nonlinear elastic-plastic analysis of innovative composite high strength steel (HSS) and geopolymer concrete (GPC) members (Fig. 1), whose merits in terms of sustainable construction are threefold. Firstly, high-strength steel with yield

[1] The University of New South Wales, UNSW Sydney, NSW, Australia.

stresses exceeding 600 MPa is used to resist the tension produced by bending action in a composite HSS-GPC member, so that the quantity of steel is reduced and subsequently less material and smaller foundations will be needed.

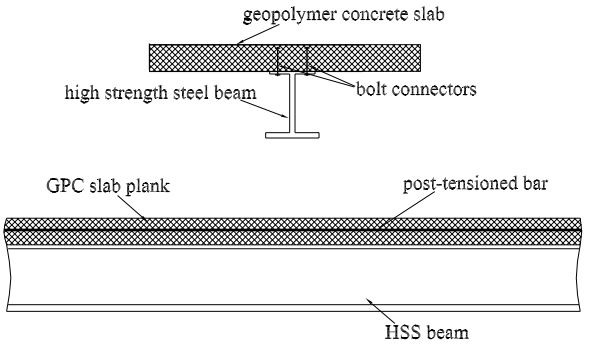

Figure 1: Cross-Section.

In addition, because the top flange of the I-section contributes little strength and stiffness to a composite member, its thickness and width can be chosen to accommodate the shear connection to the slab only, which further reduces the quantity of steel. Secondly, geopolymer concrete is used for the slab to resist the compression produced by bending action. It has been reported that the production of ordinary Portland cement currently contributes 7% to the world's carbon dioxides emissions [Davidovits (2008)] and so a reduction of this is important for environmental sustainability. Hence, it is desirable to use alternative low-emission binding agents to replace ordinary Portland cement for concrete. Geopolymers such as fly ash are an ideal replacement of the ordinary Portland cement because they are not manufactured and are 'waste' products having very good binding properties, and GPC using geopolymer as its binding agent has high compressive strength, little drying shrinkage and low creep. Applications of geopolymer concrete in composite HSS-GPC members will therefore help the reduction of carbon dioxide emissions. Thirdly, composite HSS-GPC members can be deconstructed and recycled using precast GPC planks that are post-tensioned with bars and connected to the top flange of a HSS beam by shear connection bolts (Fig. 1). This allows for potential deconstructability and recycling at the end of the life of the structure. These three attributes therefore result in a composite HSS-GPC member that is environment-friendly and which lead to a sustainable structure. However, current knowledge of the structural mechanics of composite HSS-GPC members is very limited and little research of their structural behaviour has been reported. Therefore, studies of the

structural behaviour of composite HSS-GPC members are desired for this member type to be introduced into sustainable building construction.

For this, computer modeling for the nonlinear elastic-plastic large deformation analysis of composite HSS-GPC members is needed. To meet this need, a nonlinear finite composite beam element is developed fo the modeling. In the development of the nonlinear finite composite beam element, three major problems have to be solved: geometric nonlinearity, material nonlinearity, and slip between HSS and GPC components. If the geometric nonlinearity is not treated properly, the rigid body movement may be introduced to deformations, which may lead to overstiff responses [Pi, Bradford, and Uy (2007a); Tangaramvong and Tin-Loi (2009)]. Hence, in this paper, the geometric nonlinearity is derived based on the group theory by using a special orthogonal rotation matrix to preserve scalar product of vectors, which will exclude the rigid body movements during deformation. The experimental studies of material properties of GPC reported by Hardjito, Wallah, Sumajouw, and Rangan (2005a,b), Fernandez-Jimenez, Palomo, and Lopez-Hombrados (2004), and Sofi, van Deventer, and Mendis (2007) will be used to model the material nonlinearity of GPC, while the rounded stress and strain curve proposed by Ramberg and Osgood [Lemaitre and Chaboche (1994)] will be associated with the constitutive laws of HSS. The slip between HSS and GPC components may influence the structural behavour of HSS and GPC composite members significant [He, Li, and Shang (2011)]. In addition, in the nonlinear range, the interaction between the slip and in-plane bending will produce additional shear strains and stresses at both the interface and the cross section. These shear strains and stresses associated with bolted shear connections have not been addressed numerically in the open literature. The shear stresses play a role in the local yield of the steel and concrete. Therefore, the constitutive model for the slips will be based on the slip test results of bolt connectors of Dallam (1968) and the slip will be considered as an independent degree-of-freedom in the beam element. The purpose of this paper is to combine these three essential aspects together to develop a nonlinear finite composite beam element for HSS and GPC composite members with bolted shear connections to predict their elastic-plastic large deformation behaviour, load carrying capacities and the slip between the GPC slab and the HSS beam. Th element is to be verified by comparisons with test results reported in the open literature.

2 Geometric Nonlinearity

To facilitate the development of geometric nonlinearity for the analysis of a composite HSS-GPC member, it is assumed that its deformation satisfies the Bernoulli hypothesis, i.e. its cross-sectional plane remains plane and perpendicular to the member axis during the deformation, except for slip at the interface between the

GPC slab and the HSS beam. Two axis systems are used to describe the deformation of a composite HSS-GPC member as shown in Fig. 2. The first set is a body attached (material) right-handed orthogonal axis system, which is in the position oyz in the undeformed configuration (Fig. 2) and with the axis oz being the centroidal axis of the undeformed member and the axis oy the minor principal axis of the cross-section. A unit vector $\mathbf{p}_z$ in the direction of the centroidal axis oz, and a unit vector $\mathbf{p}_y$ in the direction of the axis oy, form a right-handed orthonormal basis vector system in the axes $oxyz$ (Fig. 2). During deformation, the centroid o displaces v, w to the position o^*, the axis oz deforms into a curve, and so the body attached axis system moves and rotates to a new position $o^*y^*s^*$ as shown in Fig. 2. In a deformed configuration, a unit vector $\mathbf{q}_z$ along the tangent direction of the deformed centroidal axis o^*s^*, and the unit vector $\mathbf{q}_y$ in the direction of the minor principal axis o^*y^* of the rotated cross-section, also form an orthonormal basis vector system in the axes $o^*x^*y^*s^*$. The basis vectors $\mathbf{q}_y$, $\mathbf{q}_z$ attach to the member and move with the member during the deformation with the vector $\mathbf{q}_z$ remaining normal to the cross-section at all times.

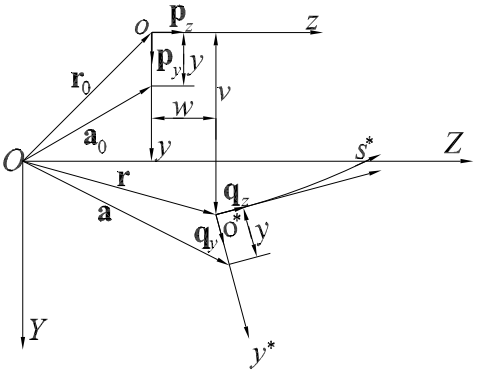

Figure 2: Position vectors.

The second set axis OXY is a space-fixed (space) right-handed rectangular coordinate system as also shown in Fig. 2. The axes OY and OZ are parallel to the axes oy and oz of the axes oyz in the undeformed configuration. The positions of the member in the undeformed and deformed configurations can be defined in the axis system OYZ.

The finite strain tensor at a material point P can be expressed as

$$\begin{bmatrix} \varepsilon_{yy} & \frac{1}{2}\gamma_{yz} \\ \frac{1}{2}\gamma_{zy} & \varepsilon_{zz} \end{bmatrix} = \frac{1}{2}(\mathbf{F}^T\mathbf{F} - \mathbf{F}_0^T\mathbf{F}_0), \tag{1}$$

where the gradient tensor $\mathbf{F}_0$ of the material point P before deformation is given by

$$\mathbf{F}_0 = \left[\frac{\partial \mathbf{a}_0}{\partial y}, \frac{\partial \mathbf{a}_0}{\partial z}\right] \tag{2}$$

while the deformation gradient tensor $\mathbf{F}$ of the material point P after the deformation is given by

$$\mathbf{F} = \left[\frac{\partial \mathbf{a}}{\partial y}, \frac{\partial \mathbf{a}}{\partial z}\right] = \left[\frac{\partial \mathbf{a}}{\partial y}, (1+\varepsilon)\frac{\partial \mathbf{a}}{\partial s}\right], \tag{3}$$

where $\mathbf{a_0}$ and $\mathbf{a}$ are the position vectors of the point P before and after deformation.

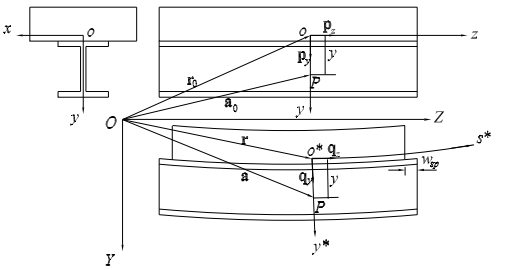

Figure 3: Slips and deformations.

The position vector $\mathbf{a}_0$ can be expressed as (Fig. 3)

$$\mathbf{a}_0 = \mathbf{r}_0 + y\mathbf{p}_y. \tag{4}$$

To consider the slip between the HSS beam and the GPC slab of a composite member, the total deformation of a material point P at a cross-section of the member results from two successive motions: translation and finite rotation of the cross-section, and a superimposed relative slip displacement between the HSS beam and the GPC slab along the unit vector $\mathbf{q}_z$ in the deformed configuration as shown in Fig. 3. Because the slip displacement $w_{sp}(z)$ is a relative axial displacement between the HSS beam and the GPC slab, its sign should be opposite for the HSS beam and the GPC slab. Under these two assumptions, the position vector $\mathbf{a}$ and , can be expressed as (Fig. 3)

$$\mathbf{a} = \mathbf{r} + y\mathbf{q}_y \mp w_{sp}(z)\mathbf{q}_z \tag{5}$$

in which the sign before the term $w_{sp}(z)\mathbf{q}_z$ is negative $(-)$ for the material point in the GPC slab and is positive $(+)$ for the material point in the HSS beam.

It is known [Pi, Bradford, and Uy (2006a, 2007a); Pi, Bradford, Tin-Loi, and Gilbert (2007b)] that for nonlinear large deformation analysis, an improper treatment of the relationship between the nonlinear strains and the displacements may lead to rigid body movements being superimposed into the finite strains, which will cause over-stiff solutions from the nonlinear analysis. From Eq. (1), it can be seen that the derivation of the finite strain tensor consists of scalar products of vectors and that to derive the finite strain tensor, the position vector $\mathbf{a}$ after deformation needs to be transformed into the two dimensional vector space formed by base vectors $\mathbf{p}_y$ and $\mathbf{p}_z$. Because any vector in the deformed configuration can be expressed by the base vectors $\mathbf{q}_y$ and $\mathbf{q}_z$, the transformation of vectors in the two dimensional vector space of deformed configuration into the two dimensional vector space of undeformed configuration reduces to the transformation from base vectors $\mathbf{q}_y$ and $\mathbf{q}_z$ to base vectors $\mathbf{p}_y$ and $\mathbf{p}_z$ as

$$\mathbf{p}_i = R_{ij}\mathbf{q}_j \quad i,j = y,z. \tag{6}$$

Group theory [Burn (2001)] shows that using the rotation matrix $\mathbf{R}$ that satisfies the orthogonal and unimodular conditions

$$\mathbf{R}^T\mathbf{R} = \mathbf{I}\ (R_{ji}R_{ij} = \delta_{ij}) \ \text{ and } \ \det\mathbf{R} = +1, \quad (\delta_{ij} \text{ is the Kronecker deltas}) \tag{7}$$

from Eq. (6), $\mathbf{q}_j = R_{ji}\mathbf{p}_i$ and the the scalar product of vectors can be preserved during rotation and so the rigid body movement can be excluded from the finite strain tensor. In fact, under the special orthogonal rotation $\mathbf{R}$, the scalar product of the vector $\mathbf{q}_j$ can be expressed as

$$\mathbf{q}_j \cdot \mathbf{q}_j = \mathbf{q}_j^T\mathbf{q}_j = (\mathbf{R}\mathbf{p}_i)^T\mathbf{R}\mathbf{p}_i = \mathbf{p}_i^T\mathbf{R}^T\mathbf{R}\mathbf{p}_i = \mathbf{p}_i^T\mathbf{p}_i = +1 \tag{8}$$

which indicates that the scalar product of vectors is preserved during the special orthogonal rotation $\mathbf{R}$.

To express the finite strain tensor as function of deformations, the special orthogonal rotation matrix $\mathbf{R}$ needs to be derived in terms of deformations. In the deformed configuration, the position vector of the centroid o^* in the fixed axis system OYZ is $\mathbf{r}$ as shown in Fig. 3, and so the vector $\mathbf{q}_z$ can be obtained by differentiating the position vector $\mathbf{r}$ of the centroid o^* with respect to the arc length s^* of the axis o^*s^* as

$$\mathbf{q}_z = \frac{\mathrm{d}\mathbf{r}}{\mathrm{d}s^*} = \frac{1}{1+\varepsilon}\frac{\mathrm{d}\mathbf{r}}{\mathrm{d}z}, \tag{9}$$

where $ds^* = (1+\varepsilon)dz$ is used, with ε being the longitudinal normal strain at the centroid defined by

$$1+\varepsilon = \sqrt{(1+w')^2+v'^2} \quad \text{with} \quad (\,)' \equiv d(\,)/dz. \tag{10}$$

In the deformed configuration, the position vector $\mathbf{r}$ of the centroid o^* can be expressed as (Fig. 3)

$$\mathbf{r} = \mathbf{r}_0 + v\mathbf{p}_y + w\mathbf{p}_z. \tag{11}$$

Substituting Eq. (11) into Eq. (9) and considering $d\mathbf{r}_0/dz = \mathbf{p}_z$ leads to

$$\mathbf{q}_z = \frac{1}{1+\varepsilon}\frac{d\mathbf{r}}{dz} = \frac{1}{1+\varepsilon}[v'\mathbf{p}_y + (1+w')\mathbf{p}_z] = \hat{v}'\mathbf{p}_y + \hat{w}'\mathbf{p}_z \tag{12}$$

where $\hat{v}' = v'/(1+\varepsilon)$, and $\hat{w}' = (1+w')/(1+\varepsilon)$, from which $\hat{v}'^2 + \hat{w}'^2 = 1$.
The rotation matrix $\mathbf{R}$ can then be expressed as

$$\mathbf{R} = \begin{bmatrix} \hat{w}' & \hat{v}' \\ -\hat{v}' & \hat{w}' \end{bmatrix}, \tag{13}$$

which can be shown to satisfy the orthogonality condition $\mathbf{R}^T\mathbf{R} = \mathbf{I}$ and the unimodular condition $\det\mathbf{R} = +1$. Hence, using the matrix $\mathbf{R}$ given by Eq. (13) to derive the finite strain tensor can exclude the rigid body movement from the finite strain tensor.

In the axis system $o^*y^*s^*$, the Frenet-Serret formula of differential geometry defines the relationship between the curvature κ and the unit vectors $\mathbf{q}_y$ and $\mathbf{q}_z$ in the deformed configuration as

$$\frac{d\mathbf{q}_y}{ds^*} = \kappa\mathbf{q}_z \quad \text{and} \quad \frac{d\mathbf{q}_z}{ds^*} = -\kappa\mathbf{q}_y, \tag{14}$$

from which the curvature κ in the deformed configuration can be obtained as

$$\kappa = \frac{d\mathbf{q}_y}{ds^*}\mathbf{q}_z = \frac{1}{(1+\varepsilon)}\frac{d\mathbf{q}_y}{dz}\mathbf{q}_z, \quad \text{or} \quad \kappa = -\frac{d\mathbf{q}_z}{ds^*}\mathbf{q}_y = -\frac{1}{(1+\varepsilon)}\frac{d\mathbf{q}_z}{dz}\mathbf{q}_y. \tag{15}$$

Substituting Eq. (6) and (13) into either equation of Eq. (15) leads to the expression for the curvature in the deformed configuration as

$$\kappa = -\frac{1}{(1+\varepsilon)}(\hat{v}''\mathbf{p}_y + \hat{w}''\mathbf{p}_z)(\hat{w}'\mathbf{p}_y - \hat{v}'\mathbf{p}_z) = \frac{\hat{v}'\hat{w}'' - \hat{w}'\hat{v}''}{1+\varepsilon}. \tag{16}$$

The finite strains can be obtained by substituting Eqs. (4) and (5) into Eq. (1) as

$$\varepsilon_{yy} = 0, \tag{17}$$

$$\varepsilon_{zz} = \frac{1}{2}\left\{[(1+\varepsilon)(1+y\kappa) \mp \tilde{w}'_{sp}]^2 + [(1+\varepsilon)\kappa\tilde{w}_{sp}]^2 - 1\right\}, \tag{18}$$

and the shear strains γ_{zy} and γ_{yz} are given as

$$\gamma_{zy} = \gamma_{yz} = \mp(1+\varepsilon)\kappa\tilde{w}_{sp}, \tag{19}$$

which are induced by the interaction between the slip and the in-plane bending. If the geometric nonlinearity is not considered, these shear strains γ_{zy} and γ_{yz} in the HSS beam and GPC slab would vanish.

3 Material Nonlinearities

3.1 Constitutive Models for Geopolymer Concrete

A finite element model for the nonlinear elastic-plastic analysis of a composite HSS-GPC member has to include the material nonlinearity of the geopolymer concrete and high strength steel. The previously formulated geometric nonlinear analysis shows that when the HSS beam and the GPC slab have partial interaction at their interface, the composite member will deform in the transverse and axial directions and that slip between the HSS beam and the GPC slab will occur. Because of this, the composite member is subjected to both bending and shear actions. Hence, the uniaxial stress-strain relationship for the GPC and HSS cannot be used directly in the nonlinear elastic-plastic analysis. Proper constitutive models for the GPC and HSS have to be established, and this section is devoted to establishing appropriate constitutive models for the GPC. In the most cases, the slab is subjected to compressive action when it forms part of a composite beam. The yield criterion for plain concrete in compression is adopted for GPC and is used in association with the uniaxial stress-strain curve of GPC; the yield criterion being expressed as [Pi, Bradford, and Uy (2006a)]

$$F_c(\sigma,\lambda) = \sigma_e^c - \sqrt{3}a_0 p^c - \sqrt{3}\tau_c = 0 \ \text{ with } \ \sigma_e^c = \sqrt{\sigma_{zz}^2 + 3\tau_{zy}^2}, \tag{20}$$

where $p^c = -\sigma_{zz}/3$ and the parameter a_0 is given by $a_0 = \sqrt{3}(1-r_{bc}^\sigma)/(1-2r_{bc}^\sigma)$, the ratio r_{bc}^σ is given by $r_{bc}^\sigma = \sigma_{bc}^u/\sigma_b^u$, with σ_{bc}^u being the ultimate stress in biaxial compression and σ_b^u being the ultimate stress in uniaxial compression, the typical value $r_{bc}^\sigma = 1.16$ is usually assumed, τ_c is a hardening parameter (τ_c is the size of the yield surface on the σ_e axis at $p^c = 0$) and in the uniaxial compression

$$\tau_c = \left(1 - \frac{a_0}{\sqrt{3}}\right)\sigma_c, \tag{21}$$

where σ_c is the magnitude of σ_{zz}.

The constitutive equation for compression of GPC can be written in an incremental form as

$$\mathrm{d}\sigma = \mathbf{E}_{ep}\mathrm{d}\varepsilon, \tag{22}$$

where the tangent material modulus matrix $\mathbf{E}^{(ep)}$ can be obtained as

$$\mathbf{E}^{(ep)} = \begin{bmatrix} E_c & 0 \\ 0 & G_c \end{bmatrix} - \frac{1}{\alpha_c}\begin{bmatrix} E_{11}^{(ep)} & E_{12}^{(ep)} \\ E_{21}^{(ep)} & E_{22}^{(ep)} \end{bmatrix} \tag{23}$$

with

$$E_{11}^{(ep)} = (\sigma_{zz} + a_0\sigma_e/\sqrt{3})^2 E_c^2,\ \ E_{12}^{(ep)} = E_{21}^{(ep)} = 3(\sigma_{zz} + a_0\sigma_e/\sqrt{3})\tau_{zy}E_cG_c \tag{24}$$

$$E_{22}^{(ep)} = 9\tau_{zy}^2 G_c^2, \quad \text{and} \quad \alpha_c = \tau_c\sigma_e^2 + E_c(\sigma_{zz} + a_0\sigma_e/\sqrt{3})^2 + 9G_c\tau_{zy}^2. \tag{25}$$

Although the GPC component is often located in the compressive zone in a composite HSS-GPC member, it may be subjected to tension in some cases such as in negative bending. Therefore, a proper model for the detection of cracking of the geopolymer concrete and a constitutive model for its tension are required. Based on plain concrete, the crack detection surface for GPC can be defined by [Pi, Bradford, and Uy (2006a)]

$$F_t = \sigma_e^t - \left(3 - b_0\frac{\sigma_t}{\sigma_t^u}\right)p^t - \left(2 - \frac{b_0}{3}\frac{\sigma_t}{\sigma_t^u}\right)\sigma_t = 0 \quad \text{with} \quad \sigma_e^t = \sqrt{\sigma_{zz}^2 + 3\tau_{zy}^2}, \tag{26}$$

where $p^t = -\sigma_{zz}/3$; $\sigma_t(\lambda_t)$ is a hardening parameter (i.e. the equivalent uniaxial tensile stress), and b_0 is a constant and its value can be obtained as

$$b_0 = 3\frac{1 + (2-f)r_t^\sigma - \sqrt{1 + (fr_t^\sigma)^2 + fr_t^\sigma}}{1 + fr_t^\sigma(1-f)} \tag{27}$$

where r_t^σ is the ratio of the ultimate stress in uniaxial tension to the ultimate stress in uniaxial compression and given by $r_t^\sigma = \sigma_t^u/\sigma_c^u$, and f is the ratio of the ultimate stress in uniaxial tension to the nonzero principal stress σ_2 at the occurrence of cracking when one principal stress has the value $\sigma_1 = \sigma_c^u$ in a plane stress test, i.e. $f = \sigma_t^u/\sigma_2$. Typical compressive yield surface defined by Eq. (20) and the crack detection surface defined by Eq. (26) are plotted together in Fig. 4.

Before cracking, the response of GPC under tensile longitudinal normal and shear stresses is assumed to be linear, and the constitutive equation can be written in an incremental form as

$$\mathrm{d}\sigma = \mathbf{E}_{ct}\mathrm{d}\varepsilon \ \text{ with } \ \mathbf{E}_{ct} = \begin{bmatrix} E_c & 0 \\ 0 & G_c \end{bmatrix}, \tag{28}$$

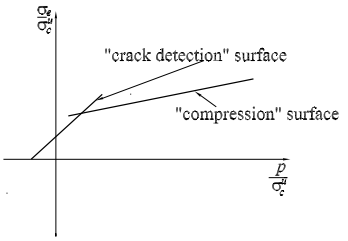

Figure 4: Proposed failure surfaces for geopolymer concrete.

in which E_c is the Young's modulus of elasticity of the concrete, G_c is the shear modulus of elasticity of the concrete and given by $G_c = E_c/[2(1+\nu_c)]$, and ν_c is the Poisson's ratio of the concrete.

After cracking, tensile stresses are generated in the cracked GPC as a result of the transfer, via shear and bond, of the stresses from the reinforcement and steel component. The Gauss point models the crack (or cracks) and the adjacent concrete and consequently its response should be stiffer than it would be for a purely brittle failure. This phenomenon is called "tension stiffening" [Gilbert and Warner (1978)]. To consider the tension stiffening, the modulus matrix $\mathbf{E}_{ct}$ in Eq. (28) is replaced by a damaged tangent material matrix $\mathbf{E}_{cr}$ given by

$$\mathbf{E}_{cr} = \begin{bmatrix} E_{cr} & 0 \\ 0 & G_{cr} \end{bmatrix}, \tag{29}$$

where E_{cr} and G_{cr} are the reduced normal and shear moduli. The reduced normal modulus can be determined by (Fig. 5)

$$E_{cr} = \frac{0 - \sigma_t^u}{\varepsilon_t^{max} - \varepsilon_t^u}, \tag{30}$$

while the shear modulus is given by

$$G_{cr} = \rho G_c, \;\; \rho = 1 - \frac{\varepsilon_t}{\varepsilon_t^{max}}, \tag{31}$$

where ε_t is the normal tensile strain and ε_t^{max} is the assumed maximum value of the normal tensile strain.

When the external load is sufficiently large, it may cause the GPC in the compressive zone to crush, and hence the constitutive model for this crushed state needs to be established. To facilitate computation after "crushing", the GPC is assumed to

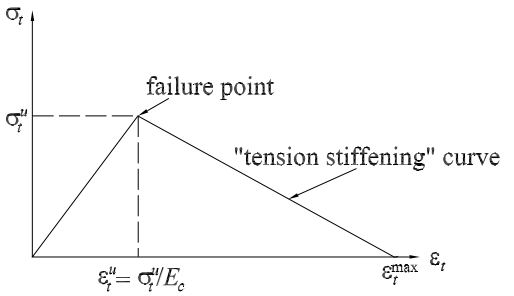

Figure 5: Tension stiffening model.

lose some, but not all, of its strength and rigidity due to the transfer of stresses from the reinforcement and the adjacent uncrushed concrete. The constitutive equation for the "crushed" concrete may be expressed as

$$\mathrm{d}\sigma = \mathbf{E}_{cr}\mathrm{d}\varepsilon \quad \text{with} \quad \mathbf{E}_{cr} = \begin{bmatrix} K & 0 \\ 0 & 0 \end{bmatrix} \quad \text{and} \quad K = \frac{E_c}{3(1-2\nu_c)} \tag{32}$$

where K is the bulk modulus of concrete.

4 Constitutive Model for High Strength Steel

The constitutive model for the nonlinearity of high strength steel is also important for the nonlinear elastic-plastic analysis of composite HSS-GPC members. Uniaxial stress-strain experiments have shown that the HSS has no typical yield stress [Lemaitre and Chaboche (1994)]. Because of this, the value of 0.2% proof stress of the uniaxial stress-strain curve of HSS is usually taken as the reference uniaxial initial yield stress. In association with the uniaxial stress-strain behaviour of HSS, the von Mises yield criterion, associated flow rule and isotropic hardening law can be used to establish the constitutive model for HSS. In this case, the von Mises yield criterion can be used to describe the change of the yield surface of HSS as

$$F = \sigma_e - \sigma_y = 0 \quad \text{with} \quad \sigma_e = \sqrt{\sigma_{zz}^2 + 3\tau_{zy}^2} \quad \text{and} \quad \sigma_y = \sigma_{0.2} + \int_0^{\varepsilon_e^{(p)}} H_s' \mathrm{d}\varepsilon_e^{(p)}, \tag{33}$$

where σ_y is the reference uniaxial yield stress, H' is the hardening parameter, $\mathrm{d}\varepsilon_e^{(p)}$ is the equivalent plastic strain rate, and $\sigma_{0.2}$ is the reference uniaxial initial yield stress.

Based on the associated flow rule and isotropic hardening law, an incremental constitutive equation for the steel can be derived as [Pi, Bradford, and Uy (2006a,b)]

$$\mathrm{d}\sigma = \mathbf{E}^{(ep)}\mathrm{d}\varepsilon \tag{34}$$

where the stress and strain increments are $\mathrm{d}\sigma = \{\mathrm{d}\sigma_{zz}, \mathrm{d}\tau_{zy}\}^T$ and $\mathrm{d}\varepsilon = \{\mathrm{d}\varepsilon_z, \mathrm{d}\gamma_{zy}\}^T$, and the tangent material modulus matrix $\mathbf{E}^{(ep)}$ is given by

$$\mathbf{E}^{(ep)} = \begin{bmatrix} E_s & 0 \\ 0 & G_s \end{bmatrix} - \frac{1}{\alpha}\begin{bmatrix} \sigma_{zz}^2 E_s^2 & 3\sigma_{zz}\tau_{zy}E_s G_s \\ 3\sigma_{zz}\tau_{zy}E_s G_s & 9\tau_{zy}^2 G_s^2 \end{bmatrix} \tag{35}$$

in which the coefficient α is given by $\alpha = \sigma_e^2 H_s' + \sigma_{zz}^2 E_s + 9\tau_{zy}^2 G_s$, E_s is the Young' modulus of elasticity, and G_s is the shear modulus of elasticity given by $G_s = E_s/[2(1+\nu_s)]$ with ν_s being the Poisson ratio of the steel.

It can also be shown [Pi, Bradford, and Uy (2007a)] that the equivalent plastic strain rate $\mathrm{d}\varepsilon_e^p$ in Eq. (33) is given by

$$\mathrm{d}\varepsilon_e^{(p)} = \mathbf{c}^T\mathrm{d}\varepsilon = \frac{\sigma_e(E_s\sigma_{zz}\mathrm{d}\varepsilon_{zz} + 3G_s\tau_{zy}\mathrm{d}\gamma_{zy})}{\sigma_e^2 H_s' + \sigma_{zz}^2 E_s + 9\tau_{zy}^2 G_s}. \tag{36}$$

5 Nonlinear Shear Force and Slip Relationship

To account for the nonlinear shear force and slip relationship, the present FE model provides a facility for the incremental relationship between the slip w_{sp} and shear force Q_{int} at the interface between the HSS beam and the GPC slab. To input the correct incremental relationship between the slip w_{sp} and shear force Q_{int} at the interface, the nonlinear shear force-slip characteristics at the interface can be obtained by push-out tests. Based on the test results, several idealized force-slip relationships such as bi-linear elastic-full plastic characteristics and rigid-plastic characteristics proposed for the design of composite members [Oehlers and Bradford (1995)] can be modified based on the push-out tests and be used for the composite GPC and HSS members. However, for the nonlinear analysis, the accuracy of the bi-linear slip and shear force relationship is not sufficient. Yam and Chapman (1968) proposed a nonlinear empirical relationship between the slip w_{sp} and the shear force Q_{int} as

$$Q_{int} = a[1 - \exp(-bw_{sp})], \tag{37}$$

where a and b are constants and they can be obtained from two points $w_{sp2} = 2w_{sp1}$ of an experimental curve as

$$a = \frac{Q_1^2}{2Q_1 - Q_2} \quad \text{and} \quad b = \frac{1}{w_{sp1}}\ln\frac{Q_1}{Q_2 - Q_1} \tag{38}$$

where Q_1 and Q_2 are the shear forces corresponding to the slips w_{sp1} and w_{sp2} respectively.

In composite HSS and GPC members, the bolt shear connectors are proposed to connect the GPC slab to the HSS beam. Dallam (1968) performed 12 push-out tests using high strength bolts with ordinary Portland concrete slabs and mild steel joists. A typical empirical curve between the slip and shear force given by Eq. (37) is compared with the push-out test results of Dallam (1968) in Fig. 6. It can be seen when the slip is small, the empirical curve agrees with the experimental results very well, but when the slip becomes large the empirical curve is somewhat conservative.

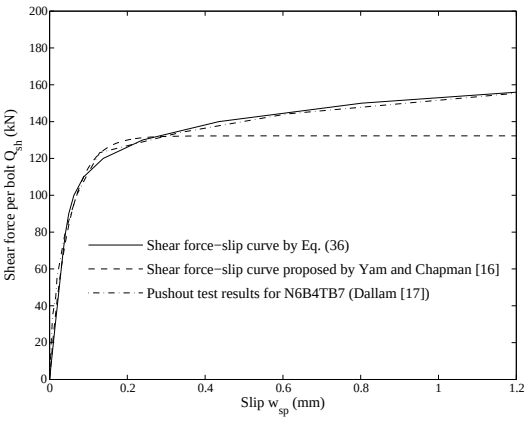

Figure 6: Nonlinear relationship between shear force and slip at interface.

For a better correlation, the new empirical relationship between the slip w_{sp} and shear force Q_{int} for the bolt shear connectors is proposed based on the test results of Dallam (1968) as

$$w_{sp} = \frac{Q_{int}}{K_l} + \frac{p}{10}\left(\frac{Q_{int}}{Q_n}\right)^c, \tag{39}$$

where K_l is the linear shear stiffness at the interface obtained from a push-out test; Q_n is the shear force at which the relationship between the slip displacement and the shear force at the interface becomes nonlinear, and which can be obtained from experiments; and the parameters p and c are chosen to match the experimental data. The empirical relationship between the slip and shear force given by Eq. (39) is also shown in Fig. 6, where $c = 10$ and $p = 10$. It can be seen that it has very good correlation with the test results of Dallam (1968).

The tangent relationship between the slip increment and the shear force increment can be obtained from Eq. (37) or Eq. (39) as

$$\mathrm{d}Q_{int} = ab\exp(-bw_{sp})\mathrm{d}w_{sp} \tag{40}$$

or

$$\mathrm{d}w_{sp} = \left(\frac{1}{K_l} + \frac{cpQ_{int}^{c-1}}{10Q_n^c}\right)\mathrm{d}Q_{int}. \tag{41}$$

To facilitate the slip displacement with the beam element, it is assumed that the shear connection between the HSS beam and the GPC slab is assumed acts as a continuous medium along the length of an element, and that the shear connectors are uniformly distributed along the length of a composite member. Hence, the shear force per unit length (shear flow force) q_{sh} can be expressed as

$$q_{int} = \frac{Q_{int}}{s} \tag{42}$$

where s is the spacing between the adjacent connectors.

Finally, the incremental relationship between the shear force per unit length q_{int} and the slip w_{sp} can be obtained from Eqs (37) (or (41)) and (42) as

$$\mathrm{d}q_{int} = K_{int}\mathrm{d}w_{sp} \tag{43}$$

where K_{int} is the tangent stiffness for the slip deformation and it can be obtained from Eq. (40) as

$$K_{int} = \frac{ab\exp(-bw_{sp})}{s}, \tag{44}$$

or from Eq. (41) as

$$K_{int} = \frac{10k_l q_n^q}{s(10Q_n^c + cpK_l Q_{int}^{c-1})}. \tag{45}$$

The incremental relationship between the shear force per unit length q_{int} and the slip w_{sp} given by Eq. (45) is used in this paper.

6 Nonlinear Equilibrium

With the nonlinear relationships for strain, displacements and slips, and the nonlinear constitutive models for the GPC and HSS, and the nonlinear slip-shear force

relationship being established, the nonlinear equilibrium equations for the elastic-plastic analysis of a composite HSS and GPC element can be derived from the principle of virtual work, which requires that

$$\delta U = \int_V \delta\varepsilon^T \sigma \mathrm{d}V + \int_0^\ell \delta w_{sp} q_{sh} \mathrm{d}z - \int_0^\ell \delta \mathbf{u}^T \mathbf{q} \mathrm{d}z - \sum_{k=1,2} \delta \mathbf{u}^T \mathbf{Q}_k = 0 \tag{46}$$

for all admissible sets of infinitesimal virtual displacements $\{\delta v, \delta w, \delta w_{sp}\}$ where ℓ is the length of the element; σ is the stress vector given by $\sigma = \{\sigma_{zz}, \tau_{zy}\}^T$; q_{sh} is the shear force per unit length; δw_{sp} is the corresponding virtual slip at the interface between the HSS and GPC components; $\mathbf{q}$ and $\mathbf{Q}_k$ are the vectors of the external distributed and concentrated loads, respectively and are given by

$$\mathbf{q} = \{q_y, q_z, m\}^T \quad \text{and} \quad \mathbf{Q}_k = \{Q_y, Q_z, M\}_k^T \ \ (k = 1, 2); \tag{47}$$

and $\delta\mathbf{u} = \{\delta v, \delta w, -\delta v'\}^T$ is the vector of the virtual displacements conjugate to the load vectors $\mathbf{q}$ and $\mathbf{Q}_k$; and the virtual strain $\delta\varepsilon = \{\delta\varepsilon_{zz}, \delta\gamma_{zy}\}^T$ can be expressed as

$$\delta\varepsilon = \mathbf{S}\mathbf{B}\delta\mathbf{d} \tag{48}$$

with the matrix $\mathbf{S}$ being given by

$$\mathbf{S} = \begin{bmatrix} 1 & y & 0 \\ 0 & 0 & 1 \end{bmatrix}, \tag{49}$$

the vector of general displacements given by

$$\mathbf{d} = \{v, v', v'', w, w', w'', w_{sp}, w'_{sp}\}^T, \tag{50}$$

and the matrix $\mathbf{B}$ given by

$$\mathbf{B} = \begin{bmatrix} 0 & v' & 0 & 0 & 1+w' & 0 & 0 & w_{sp} \mp 1 \\ 0 & w'' & -(1+w' \mp w'_{sp}) & 0 & -v'' & v' & 0 & \pm v'' \\ 0 & 0 & \mp w_{sp} & 0 & 0 & 0 & \mp v'' & 0 \end{bmatrix}. \tag{51}$$

By substituting Eq. (48) into the virtual work given by Eq. (46) and expressing the general displacement vector as $\mathbf{d} = \mathbf{N}\mathbf{r}$, where $\mathbf{N}$ is the shape function matrix whose elements are functions of z, and $\mathbf{r}$ is the nodal displacement vector given by

$$\mathbf{r}^T = \{v_1, v'_1, w_1, w'_1, w_{sp1}, w'_{sp1}, v_2, v'_2, w_2, w'_2, w_{sp2}, w'_{sp2}\}, \tag{52}$$

the nonlinear equilibrium equations can be derived as

$$\mathbf{p}_{in} = \mathbf{p}, \tag{53}$$

where $\mathbf{p}_{in} = \int_0^\ell \mathbf{N}^T(\mathbf{B}^T\mathbf{R} + \mathbf{q}_{sh})\mathrm{d}z$ and $\mathbf{p} = [\int_0^\ell \mathbf{N}^T\mathbf{A}^T\mathbf{q}\mathrm{d}z + \sum_{k=1,2}\mathbf{N}^T\mathbf{A}^T\mathbf{Q}_k]$ are vectors of the internal and external forces respectively, in which $\mathbf{R}$ is the vector of the stress resultants given by $\mathbf{R} = \int_A \mathbf{S}^T\sigma\mathrm{d}A$, $\mathbf{q}_{sh}$ is an 8×1 vector of the unit shear force acting at the interface between steel and concrete components and given by $\mathbf{q}_{sh} = \{0,0,0,0,0,0,q_{sh},0\}^T$ with q_{sh} being given by Eq. (43), and $\mathbf{A}$ is a 3×8 matrix and its non-zero elements are given by $A_{11} = 1$, $A_{22} = -1$ and $A_{33} = 1$.

7 Incremental Equilibrium

Applying the principle of virtual work to successive equilibrium states defined by ($\mathbf{q}$, $\mathbf{Q}$ δ), and ($\mathbf{q}+\Delta\mathbf{q}$, $\mathbf{Q}+\Delta\mathbf{Q}$,$\delta+\Delta\delta$) leads to

$$\left\{\frac{\mathrm{d}(\delta U)}{\mathrm{d}\delta}\right\}^T \Delta\delta + \left\{\frac{\mathrm{d}(\delta U)}{\mathrm{d}\mathbf{q}}\right\}^T \Delta\mathbf{q} + \sum_{k=1,2}\left\{\frac{\mathrm{d}(\delta U)}{\mathrm{d}\mathbf{Q}_k}\right\}^T \Delta\mathbf{Q}_k = 0. \tag{54}$$

Substituting Eq. (46) into Eq. (54) and considering that the elements of the matrix $\mathbf{A}$ are constants and so $\mathrm{d}\mathbf{A} = \mathbf{0}$ leads to the incremental equations of equilibrium as

$$\mathbf{k}_T\Delta\mathbf{r} = \Delta\mathbf{p}, \tag{55}$$

where the tangent stiffness matrix $\mathbf{k}_T$ is given by

$$\mathbf{k}_T = \int_0^\ell \mathbf{N}^T(\mathbf{B}^T\mathbf{D}\mathbf{B} + \mathbf{M}_\sigma + \mathbf{M}_{sh})\mathbf{N}\mathrm{d}z, \tag{56}$$

and the vector of equivalent external incremental loads $\Delta\mathbf{p}$ is given by

$$\Delta\mathbf{p} = \int_0^\ell \mathbf{N}^T\mathbf{A}^T\Delta\mathbf{q}\mathrm{d}z + \sum_{i=1,2}\mathbf{N}^T\mathbf{A}^T\Delta\mathbf{Q}_k. \tag{57}$$

In Eq. (56), the matrix $\mathbf{M}_\sigma$ is an 8×8 symmetric matrix that accounts for the nonlinear effects of the stress resultants on the tangent stiffness matrix, the matrix $\mathbf{M}_{sh}$ is an 8×8 matrix with elements $M_{sh}(i,j) = \delta_{7,j}\delta_{i,7}K_{sh}$ in which $\delta_{i,j}$ is the Kronecker delta ($\delta_{i,j} = 1$ when $i = j$ and $\delta_{i,j} = 0$ when $i \neq j$) and K_{sh} is given by Eq. (43), and the matrix $\mathbf{D}$ is given by

$$\mathbf{D} = \int_A \mathbf{S}^\mathbf{T}\mathbf{E}^{ep}\mathbf{S}\mathrm{d}A. \tag{58}$$

8 Incremental-Iterative Analysis

A Newton-Raphson method is used in conjunction with the incremental equilibrium equations given by Eq. (55) to solve the nonlinear equilibrium equations (53). In

the incremental-iterative implementation, each load step consists of the application of an increment of the external loads and subsequent iterations to correct the errors until the nonlinear equilibrium governed by Eq. (53) is restored within a specified admissible tolerance. Before the restoration, the internal and external forces are not in equilibrium and hence the incremental-iterative equilibrium equations can be written from Eq. (55) as

$$\mathbf{k}_i \Delta \mathbf{r}_i^j = \Delta \mathbf{p}_i - \Delta \mathbf{p}_i^{j-1}, \tag{59}$$

where i and j denote the load step and the iteration within the load step, respectively, and $\Delta \mathbf{p}_i^{j-1}$ is the unbalanced force in the last iteration $(j-1)$ that can be calculated using Eq. (53) as

$$\Delta \mathbf{p}_i^{j-1} = [\mathbf{p}_{in} - \mathbf{p}]_i^{j-1}. \tag{60}$$

The arc-length method is used as the iterative strategy, with an automatic increment of the arc-length being used [Pi, Bradford, and Uy (2007a)]. The sign of the determinant of the tangent stiffness matrix is used for the sign of the load increment. The maximum norm of the incremental displacements is used for testing the convergence, so that

$$||\varepsilon|| = \max_k |\frac{\Delta r_k}{r_{k,ref}}| < \zeta \tag{61}$$

where Δr_k is the change in the displacement component k during the current iteration cycle, $r_{k,ref}$ is the largest displacement component of the corresponding type, and ζ is in the range 10^{-2} to 10^{-5}, depending on the desired accuracy.

During the incremental-iterative solution, the incremental general displacements instead of the iterative general displacements are used to calculate the strain increments and strain updating, so that "spurious unloading" can be avoided. The elastic predictor and radial return technique [Zienkiewicz and Taylor (1989)] is adopted in the strain-stress incremental calculation.

9 Applications

9.1 General

In the implementation of the FE program, the constitutive models for the geopolymer concrete and high strength steel need to be used in association with their uniaxial stress-strain curves. The stress-strain curve for GPC is somewhat different from that of ordinary Portland concrete, as found by Davidovits (2008), and Hardjito, Wallah, Sumajouw, and Rangan (2005a). They used uniaxial stress-strain curve as

$$\sigma = \frac{\sigma_{max}}{\varepsilon_{max}} \frac{n\varepsilon}{n-1+(\varepsilon/\varepsilon_{max})^{nk}} \tag{62}$$

where σ_{max} and ε_{max} are the peak stress and the strain corresponding to the peak stress, the parameter n is defined as $n = 0.8 + (\sigma_c/12)$, and the parameter k is defined as

$$k = \begin{cases} 0.67 + (\sigma_{max}/62) & \varepsilon/\varepsilon_{max} > 1 \\ 1 & \varepsilon/\varepsilon_{max} \leq 1 \end{cases} . \tag{63}$$

The formula for the elastic modulus of geopolymer concrete was also proposed by Davidovits (2008) and Hardjito, Wallah, Sumajouw, and Rangan (2005a) as

$$E_c = (5300 + 2707\sqrt{f'_c})(\text{MPa}). \tag{64}$$

Eq. (62) and (64) are used in this paper for GPC and a typical stress-strain curve for GPC is shown in Fig. 7.

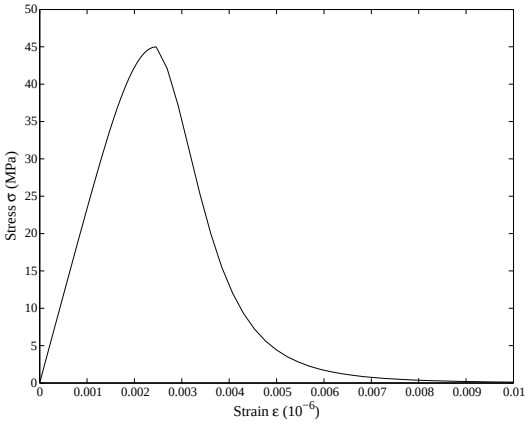

Figure 7: Stress-strain curve for geopolymer concrete.

For the HSS, the rounded stress and strain curve proposed by Ramberg and Osgood [Lemaitre and Chaboche (1994)] is used, which is expressed as

$$\varepsilon = \frac{\sigma}{E_s} + \frac{p}{100}\left(\frac{\sigma}{\sigma_p}\right)^n, \tag{65}$$

where E_s is the Young's modulus of elasticity, σ_p is a reference stress and usually takes the value of the 0.2% proof stress, i.e., $\sigma_p = \sigma_{0.2}$, and the parameters p and n are chosen to match the test data. A typical stress-strain curve is shown in Fig. 8.

The FE model of this paper can also be used for the nonlinear elastic-plastic analysis of the conventional composite steel and concrete members. In this case, the

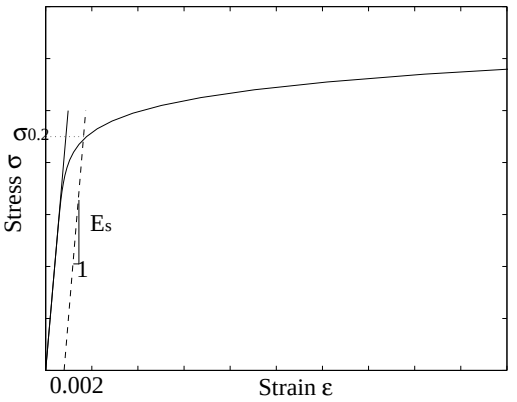

Figure 8: Stress-strain curve for high strength steel.

tri-linear stress-strain curve is used for the mild steel, while the following stress-strain curve is used for the normal concrete [Pi, Bradford, and Uy (2006a)]

$$\sigma = \frac{E_c \varepsilon}{1 + [E_c/(\sigma_c/\varepsilon_c) - 2]\varepsilon/\varepsilon_c + (\varepsilon/\varepsilon_c)^2} \tag{66}$$

where σ_c is the maximum compressive stress and ε_c is the strain corresponding to σ_c.

The accuracy of the incremental-iterative plastic analysis is related not only to the algorithm used, but also to the sampling point scheme over the cross-section that should be chosen in the most appropriate way. In order to determine the correct stress state over the entire cross-section and to detect the cracking and crushing of the concrete correctly, a composite cross-section needs to be divided into several components so as to use the corresponding material properties and constitutive models. Each of the components of the composite cross-section are further divided into a number of areas. The non-bias Gaussian numerical integration technique [Zienkiewicz and Taylor (1989)] is used in the present FE model. The number of areas and the number of Gaussian points in each area can be determined in accordance to the problem in hand.

9.2 Composite beams tested by Dallam (1968)

Because the use of composite HSS-GPC members in construction is relatively new proposal, the analytical, numerical and experimental studies on their structural behaviour do not appear to have been reported in the open literature. Hence, the finite beam element developed in this paper is used to analyze the bolted composite steel and concrete beams tested by Dallam (1968) at the University of Missouri

in 1968. They carried out static tests of six full-scale simply-supported composite beams using high-strength bolts as shear connectors. The bolts were placed through pre-drilled holes in the top flange of the steel beam and were tensioned after the concrete had cured. The six full-scale composite beams were tested in two series and each series consists of three beams. The dimensions, the cross-section, and the loadings of the first and second series are shown in Figs. 9(a) and 9(b) respectively. Eight beam elements were used to model the composite beams. The

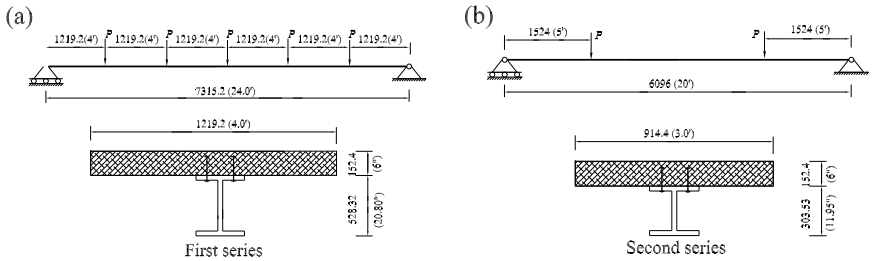

Figure 9: Composite beam tested by Dallam (1968).

strength and Young's modulus of the steel beams obtained from the experiments are shown in Table 1, while the compressive strength, unit weight, and Young's modulus of the concrete slab are shown in Table 2. In the FE computation, the shear force-slip relationships given by Eq. (43) with appropriate parameters obtained from the push-out test results of Dallam and Harpster (1968) were used.

Table 1: Young's modulus and strength of steel

Specimen	Young's Modulus E_s		Strength σ_s			
			Web		Flange	
	Psi$\times 10^6$	MPa	Psi$\times 10^3$	MPa	Psi$\times 10^3$	MPa
NFB4B2	29.0	199,955	38.0	262.01	36.6	252.36
NFB6B2	29.1	200,644	38.2	263.39	37.2	256.49

The FE results of variations of the central deflection v_c with the load per jack P are compared with test results of Dallam and Harpster (1968) in Fig. 10(a) for the composite beams NFB6B2 of the first series, and in Fig. 10(b) for NFB4B2 of the second series, respectively. For the beam NFB6B2 (Fig. 10(a)), the nonlinear behaviour starts at the load $P = 140$ kN. As the load increases, the yielding increases and spreads to other section of the beam. As the load increases above $P = 205$kN, the composite beam fails by crushing the concrete of the slab at the centre of the

Table 2: Young's modulus, strength and unit weight of concrete

Specimen	Young's Modulus E_c		Compressive Strength σ'_c		Unit Weight	
	Psi$\times 10^6$	MPa	Psi$\times 10^3$	MPa	Pcf	kg/m^3
NFB4B2	4.19	28,890	6.89	47.51	137.5	2195
NFB6B2	4.57	31,510	7.13	49.16	144.0	2307

1 Psi$\times 10^3$=1kip/in^2 = 6.895MPa, 1 Pcf = 16.0187kg/m^3

beam. For the beam NFB4B2 (Fig. 10(b)), the steel beam began to yield at the load $P = 150$ kN. As the load increases above $P = 210$kN, the composite beam fails by crushing the concrete of the slab at the centre of the beam. It can be seen that the agreement of the FE results with the test results is very good.

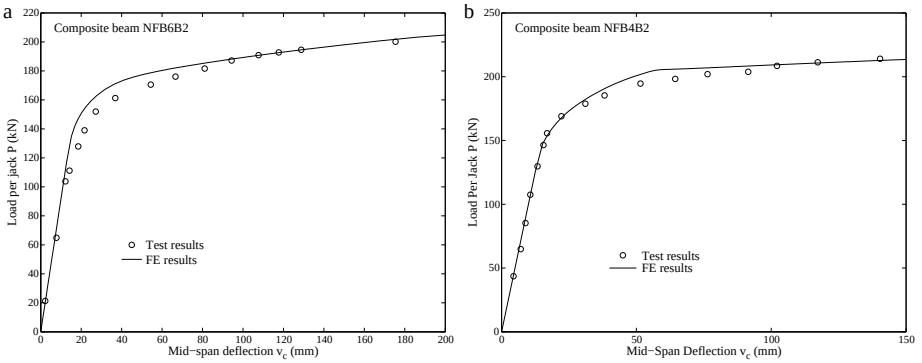

Figure 10: Comparison with test results for mid-deflection of beams NFB6B2 and NFB4B2 [Dallam (1968)].

The FE results for the end slips are also compared with the test results as the variations of the end slip with the load per jack in Fig. 11(a) for the beam NFB6B2, and in Fig. 11(b) for the beam NFB4B2. It can be seen that the agreement of the FE results with the test results is also very good.

9.3 Geopolymer reinforced concrete columns tested by Sumajouw, Hardjito, Wallah, and Rangan (2007)

To verify that the material properties of GPC are properly formulated in the FE program developed in this paper, the FE program was used to perform the nonlinear elastic-plastic analysis of geopolymer reinforced concrete columns tested by Sumajouw, Hardjito, Wallah, and Rangan (2007), who performed tests of 12 geopolymer

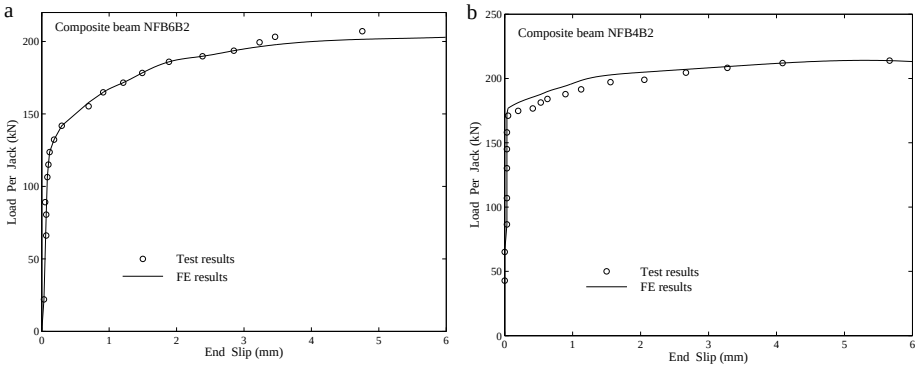

Figure 11: Comparison with test results for end slip of beams NFB6B2 and NFB4B2 [Dallam (1968)].

reinforced columns. The cross-section of the columns is shown in Fig. 12. The longitudinal reinforcement of the columns consists of 4 or 8 Australian N12 deformed steel bars. The nominal cross-sectional area of an N12 bar is 110mm^2 and the yield stress was obtained in the tensile test as 519 MPa. The lateral closed ties consist of 6 mm diameter (W6) hard-drawn steel wires at 100 mm spacing. The cylinder strength of each tested column obtained from the cylinder crushing test is listed in Table 3.

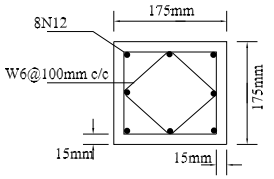

Figure 12: GPC columns tested by Sumajouw, Hardjito, Wallah, and Rangan (2007).

However, the strength of concrete in a column differs from that in the cylinder test due to their differences in size, vibration during casting, curing, loading rate etc. To take these differences into account, a factor k_3 is applied to the cylinder stress to obtain the concrete strength for the corresponding column. ACI Committee 263 (1984) recommended $k_3 = 0.85$. Ibrahim and MacGregor (1997) showed the value of k_3 varies from 0.82 to 1.12 for the concrete with σ_c of 40-120 MPa. MacGregor and Wight (2006) proposed $k_3 = 0.9$. The value of $k_3 = 0.9$ is used in the FE

Table 3: Details of GPC columns

Specimen	Cylinder Strength f'_c (MPa)	Longitudinal reinforcement	e (mm)
GCI-1	42	4B12	15
GCI-2	42	4N12	35
GCI-3	42	4N12	50
GCI-4	43	8N12	15
GCI-5	43	8N12	35
GCI-6	43	8N12	50
GCII-1	66	4N12	15
GCII-2	66	4N12	30
GCII-3	66	4N12	50
GCII-4	59	8N12	15
GCII-5	59	8N12	30
GCII-6	59	8N12	50

analysis for these geopolymer reinforced columns to account for the difference between the GPC strength of the columns and the GPC cylinder strength.

The stress-strain relationship given by Eq. (62) is used in association with the tested properties of the GPC given in Table 3. Since the elastic modulus of the GPC was not reported, the formula proposed by Hardjito, Wallah, Sumajouw, and Rangan (2005a) and given by Eq. (64) was used for calculation of the elastic modulus. Eight elements were used for each column.

The FE results for typical variations of the mid-height deflection with the external load are shown in Fig. 13 for the GPC reinforced columns GCI1-1, GCI1-5 and GCI1-6. It can be been the FE results agree with the test results very well.

The FE results for the ultimate load and the corresponding mid-height deflection of all tested columns are compared with the test results in Table 4. The mean value of the ratio of the FE and test results for the ultimate loads of the 12 columns is 1.015, while the mean value of the ratio of the FE and test results for mid-height deflections at the ultimate loads of the 12 columns is 1.017.

9.4 Continuous composite beam tested by Ansourian (1981)

Six continuous composite steel-concrete beams using ordinary concrete were tested by Ansourian (1981) and are widely-used for benchmark data. The tested beams CTB2 and CTB5 (Fig. 14) are herein used to demonstrate the ability of the present FE model in analyzing the nonlinear elastic-plastic behaviour of the continuous composite steel-concrete beams.

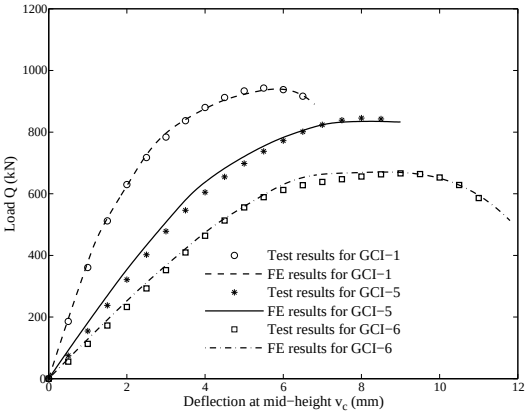

Figure 13: Comparison with test results for mid-deflection of GPC columns.

Table 4: Comparison with test results of Sumajouw, Hardjito, Wallah, and Rangan (2007)

Specimen	Test results		FE results		Correlation	
	Q_{max}(kN)	v_c (mm)	Q_{max}(kN)	v_c (mm)	Q_{max}(kN)	v_c (mm)
GCI-1	940	5.44	937	5.58	0.9968	1.0257
GCI-2	674	8.02	720	8.41	1.0682	1.0486
GCI-3	555	10.31	534	10.82	0.9622	1.0495
GCI-4	1,237	6.24	1,226	6.03	0.9911	0.9663
GCI-5	852	9.08	864	8.87	1.0141	0.9515
GCI-6	666	9.40	675	9.62	1.0135	1.0244
GCII-1	1,455	4.94	1,376	5.53	0.9457	1.1194
GCII-2	1,030	7.59	1,032	7.94	1.0019	1.0461
GCII-3	827	10.70	886	9.91	1.0713	0.9262
GCII-4	1,559	5.59	1,561	6.38	1.0013	1.1413
GCII-5	1,057	7.97	1,100	7.37	1.0407	0.9247
GCII-6	810	9.18	869	9.04	1.0728	0.9847
Mean					1.015	1.017

The dimensions of the steel I-section of CTB2 and CTB5 are: the overall depth $d = 200$ mm, the web thickness $t_w = 5.6$ mm, the flange width $b_f = 100$ mm, and the flange thickness $t_f = 8.5$ mm for CTB2, and $d = 240$ mm, $t_w = 6.2$ mm, $b_f = 100$ mm, and are: $t_f = 9.8$ mm for CTB5. The Young's moduli of the steel and concrete are assumed as $E_s = 200,000$ MPa and $E_c = 28,869$ MPa. The stress-

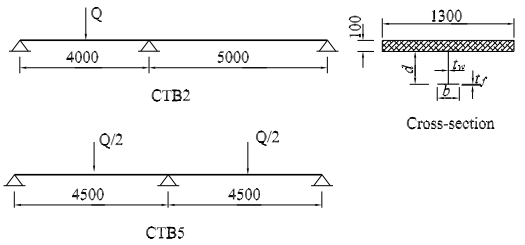

Figure 14: Continuous composite steel-concrete beams tested by Ansourian (1981).

strain curve for conventional concrete given by Eq. (66) was used for the concrete slabs with 200 mm cube strength 50 MPa for CTB2, and 29 MPa for CTB5. Tri-linear stress-strain curve was used for the steel I-beam and reinforcement with the initial yield stresses 277 MPa, 340 MPa, and 430 MPa for the flange, web and reinforcement of CTB2, and 265 MPa, 278 MPa, and 430 MPa for the flange, web and reinforcement of CTB5. The FE results for variations of the applied load with the vertical deflections of the middle spans are compared with the test results in Fig. 15(a) for the beam CTB2, and in Fig. 15(b) for the beam CTB5. Eight elements were used for each beam. The FE results agrees with the test results very well.

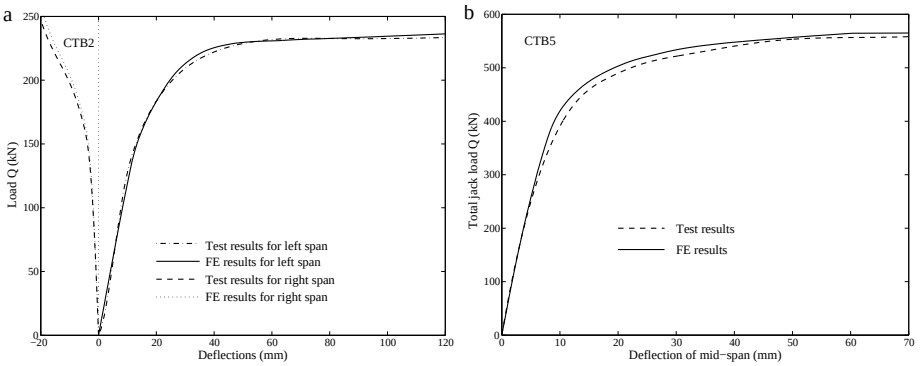

Figure 15: Comparison with test results of Ansourian (1981).

10 Conclusions

This paper has developed a finite composite beam element for the nonlinear elastic-plastic analysis of composite HSS and GPC members. The relative slip between the steel and concrete components was considered as an independent degree-of-

freedom. The geometric nonlinearities were derived using vector analysis and differential geometry to exclude rigid body movements from the nonlinear strains. Constitutive models for the compression, crack detection, and crushing of geopolymer concrete were proposed to account for the material nonlinearity of geopolymer concrete. In the FE implementation, these constitutive models were used in association with the uniaxial stress-strain curve for geopolymer concrete proposed by Hardjito, Wallah, Sumajouw, and Rangan (2005a, 2004). The effects of nonlinearities and slip on the deformations and strains in the steel and concrete components and so on the stress resultants, stiffness, and strength of the composite member are thus combined together in the FE formulation. The comparisons reported with the experimental results demonstrated the good numerical capacity and efficiency of the nonlinear finite beam element developed in this paper.

Acknowledgement: This work has been supported by the Australian Research Council through a Laureate Fellowship (FL100100063) awarded to the first author and Discovery Projects (DP1097096 and DP1096454) awarded to both authors.

References

ACI Committee 263 (1984): State of the art report on high strength concrete. *ACI Proceedings*, vol. 81, no. 4, pp. 364–411.

Ansourian, P. (1981): Experiments on continuous composite beams. *Proceedings of Institution of Civil Engineers*, vol. 71, no. Part 2, pp. 25–71.

Burn, R. P. (2001): *Groups. A path to geometry*. Cambridge, University Press.

Dallam, L. N. (1968): Pushout tests with high strength bolt shear connectors. Report 68-7, Department of Civil Engineering, University of Missouri, USA, 1968.

Dallam, L. N.; Harpster, J. L. (1968): Composite beam tests with high-strength bolt shear connectors. Report 68-3, Department of Civil Engineering, University of Missouri, USA, 1968.

Davidovits, J. (2008): *Geopolymer Chemistry and Applications*. Institute G*é*opolym*è*r, Saint-Quentin, France.

Fernandez-Jimenez, A. M.; Palomo, A.; Lopez-Hombrados, C. (2004): Engineering properties of alkali-activated fly ash concrete. *ACI Material Journal*, vol. 103, no. 2, pp. 106–112.

Gilbert, R. I.; Warner, R. F. (1978): Tension stiffening in reinforced concrete slabs. *Journal of the Structural Division ASCE*, vol. 104, no. ST12, pp. 1885–1900.

Hardjito, D.; Wallah, S. E.; Sumajouw, D. M. J.; Rangan, B. V. (2004): On the development of fly ash-based geopolymer concrete. *ACI Material Journal*, vol. 101, no. 6, pp. 467–472.

Hardjito, D.; Wallah, S. E.; Sumajouw, D. M. J.; Rangan, B. V. (2005a): The stress-strain behaviour of fly ash-based geopolymer concrete. In *Development in mechanics of structures and material*, pp. 831–834. A Balkema Publishers, The Netherlands.

Hardjito, D.; Wallah, S. E.; Sumajouw, D. M. J.; Rangan, B. V. (2005b): Fly ash-based geopolymer concrete. *Australian Journal of Structural Engineering*, vol. 6, no. 1, pp. 77–86.

He, S.; Li, P.; Shang, F. (2011): Three-dimensional simulation of the shear properties of steel-concrete composite beams using an interface slip model. *CMES-Computer Modeling in Engineering & Sciences*, vol. 73, no. 4, pp. 387–394.

Ibrahim, H. H.; MacGregor, J. G. (1997): Modification of the aci rectangular stress block for high-strength concrete. *ACI Structural Journal*, vol. 94, no. 1, pp. 40–48.

Lemaitre, L.; Chaboche, J.-L. (1994): *Mechanics of solid materials*. Cambridge University Press, Cambridge, UK.

MacGregor, J. G.; Wight, J. K. (2006): *Reinforced Concrete Mechanics and Design, 4th edition, In SI units*. Prentice hall, Singapore.

Oehlers, D. J.; Bradford, M. A. (1995): *Composite steel and concrete structural members. Fundamental behaviour*. Pergamon, Oxford, UK.

Pi, Y.-L.; Bradford, M. A.; Tin-Loi, F.; Gilbert, R. I. (2007b): Geometric and material nonlinear analysis of elastically restrained arches. *Engineering Structures*, vol. 29, no. 3, pp. 283–295.

Pi, Y.-L.; Bradford, M. A.; Uy, B. (2006a): Second order nonlinear inelastic analysis of composite steel-concrete members. I: Theory. *Journal of the Engineering Mechanics Division ASCE*, vol. 132, no. 5, pp. 751–761.

Pi, Y.-L.; Bradford, M. A.; Uy, B. (2006b): Second order nonlinear inelastic analysis of composite steel-concrete members. II: Applications. *Journal of the Engineering Mechanics Division ASCE*, vol. 132, no. 5, pp. 762–771.

Pi, Y.-L.; Bradford, M. A.; Uy, B. (2007a): A rational elasto-plastic spatially curved thin-walled beam element. *International Journal for Numerical Methods in Engineering*, vol. 70, no. 3, pp. 253–290.

Sofi, M.; van Deventer, J. S. J.; Mendis, P. A. (2007): Engineering properties of inorganic polymer concretes (ipcs). *Cement Concrete Research*, vol. 37, pp. 251–257.

Sumajouw, D. M. J.; Hardjito, D.; Wallah, S. E.; Rangan, B. V. (2007): Fly ash-based geopolymer concrete: study of slender columns. *Journal of Material Sciences*, vol. 42, no. 9, pp. 3124–3130.

Tangaramvong, S.; Tin-Loi, F. (2009): Extended limit analysis of atrain aoftening frames involving 2nd-order geometric nonlinearity and limited ductility. *CMES-Computer Modeling in Engineering & Sciences*, vol. 42, no. 3, pp. 217–256.

Yam, L. C. P.; Chapman, J. C. (1968): The inelastic behaviour of simply supported composite beams of steel and concrete. *Proceedings of Institution of Civil Engineers*, vol. 41, no. 2, pp. 651–683.

Zienkiewicz, O. C.; Taylor, R. L. (1989): *The Finite Element Method, 4th edition*. McGraw-Hill, New York, NY, USA.